Eur. Phys. J. B **14**, 655–659 (2000)

THE EUROPEAN PHYSICAL JOURNAL B

EDP Sciences

Magnetic properties of the S = 1/2 one-dimensional antiferromagnet $MgVO_3$

J. Choukroun[1], V.A. Pashchenko[2], Y. Ksari[1], J.Y. Henry[3], F. Mila[4], P. Millet[5], P. Monod[6], A. Stepanov[1,a], J. Dumas[7], and R. Buder[7]

[1] Laboratoire MATOP, Université d'Aix-Marseille III and CNRS, Faculté des Sciences de Saint-Jérôme, C-151, 13397 Marseille Cedex 20, France
[2] Grenoble High Magnetic Field Laboratory, MPI–FKF and CNRS, 38042 Grenoble Cedex 9, France
[3] CEA Grenoble, Département de Recherche Fondamentale sur la Matière Condensée, 38054 Grenoble Cedex 9, France
[4] Laboratoire de Physique Quantique, Université Paul Sabatier and CNRS, 118 route de Narbonne, 31062 Toulouse, France
[5] Centre d'Élaboration de Matériaux et d'Études Structurales, CNRS, BP 4347, 29 rue J. Marvig, 31055 Toulouse Cedex 4, France
[6] Laboratoire de Physique de la Matière Condensée, ENS, 24 rue Lhomond, 75231 Paris Cedex 5, France
[7] Laboratoire d'Études des Propriétés Électroniques des Solides, CNRS, 38042 Grenoble Cedex 9, France

Received 14 July 1999

Abstract. The magnetic susceptibility and the electron spin resonance in the X-band of the transition metal oxide compound $MgVO_3$ are reported. We show that this compound, made of weakly coupled infinite chains of VO_5 pyramids, behaves as a $S = 1/2$ one-dimensional Heisenberg antiferromagnet. From the ESR and magnetic experiments we deduce the Néel temperature $T_N = 5.2 \pm 0.5$ K, the in-chain coupling constant $J/k = 100 \pm 5$ K and the g-factor values $g_x = g_z = 1.972(2)$, $g_y = 1.946(1)$ for V^{4+} ions in $MgVO_3$.

PACS. 75.30.Et Exchange and superexchange interactions – 75.30.Cr Saturation moments and magnetic susceptibilities – 75.40.-s Critical-point effects, specific heats, short-range order

1 Introduction

During the latest decades, a large amount of theoretical as well as experimental work has been devoted to the study of low dimensional magnetic materials [1,2]. Since the Haldane's prediction, stating a differentiation between integer and half integer spin systems [3], a particular attention was paid to one-dimensional (1D) quantum antiferromagnets ($S = 1/2$, $S = 1$). More recently, other quantum Heisenberg systems such as ladders and planes have also been investigated [4]. If there are already good experimental realizations of some of the previously mentioned models, there is a clear need of new compounds to study all the aspects of the problem.

In that respect, vanadium oxides are currently the center of much attention since they often lead to $S = 1/2$ or $S = 1$ systems with reduced dimensionality. α'-NaV_2O_5 is currently intensively studied because it is thought that this compound belongs to the class of Spin-Peierls systems [5,6]. $(VO)_2P_2O_7$ [7], first believed to realize a ladder model where the longitudinal coupling J is comparable to the coupling J' along the rungs, is now thought to be closer to a dimerized Heisenberg model [8]. Recently, it has been proposed that in CaV_2O_5 [9] and MgV_2O_5 [10], the spins are arranged in planes made of coupled ladders. Finally CaV_4O_9 is the first example of a quasi-2D spin system with a spin gap [11]. In this communication we report the first magnetic and X-band ESR measurements on $MgVO_3$. We show that this compound is a quasi-1D antiferromagnet ($S = 1/2$) with a coupling along the chains $J/k = 100 \pm 5$ K and that it orders antiferromagnetically at $T_N = 5.2 \pm 0.5$ K.

2 Structure

The first structural determination of $MgVO_3$ was reported by Bouloux, Milosevic and Galy [12]. This compound crystallizes in the orthorhombic system and the last refinement indicates that the space group is Cmcm ($a = 0.5287(1)$ nm, $b = 1.0030(2)$ nm, $c = 0.5239(1)$ nm) rather than $Cmc2_1$. The structure consists of sheets of edge sharing square pyramids having their basal face parallel to the (010) plane and their apices pointing alternatively below and above this plane (see Fig. 1). From a magnetic point of view, the structure can be viewed as a sequence of infinite chains of VO_5 pyramids running along the [001] direction and isolated magnetically by infinite

[a] e-mail: stepanov@matop.u-3mrs.fr

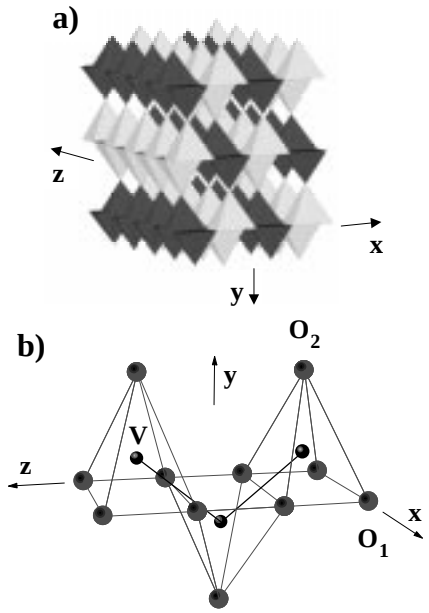

Fig. 1. (a) Perspective view of the structure of $MgVO_3$. The chains of square pyramids occupied by V^{4+} and Mg^{2+} are in black and gray, respectively. (b) Schematic representation of an isolated VO_5 chain in $MgVO_3$.

chains of MgO_5 pyramids (Fig. 1a). The unit cell contains 4 V^{4+} ions, each carrying a spin 1/2. The choice of the space group Cmcm results in very regular square pyramids with four distances V-O_1 and Mg-O_1 equal respectively to 1.946(2) Å and 2.038(2) Å and short distances V-O_2 and Mg-O_2 equal to 1.633(5) Å and 1.963(5) Å. This type of coordination for vanadium 4+ is commonly encountered in vanadium oxides, some of which, as said in the introduction, are currently studied intensively because of the richness of the magnetic phenomena they exhibit. The smallest in-chain V^{4+}-V^{4+} distance is 2.960(8) Å, a value much smaller than the smallest chain-to-chain V^{4+}-V^{4+} distance of 5.204 (1) Å. Figure 1b shows in more detail the structure of the magnetic V^{4+} chain in $MgVO_3$ and the distribution of the oxygen atoms around V^{4+} ions.

3 Experimental conditions

Polycrystalline $MgVO_3$ was prepared starting from a stoichiometric mixture of MgO, V_2O_3 and V_2O_5, sealed in an evacuated quartz tube, heated at 940 °C during 15 hours and then furnace cooled. Single crystals were obtained by rapidly heating (15 minutes) the previous mixture to 1150 °C where it was kept for 30 min, and then cooling it slowly (10 °C/h) down to 940 °C. The red-brown colored crystals of a typical size of $1 \times 0.5 \times 0.05$ mm^3 could be removed from the mixture after furnace cooling.

No impurity phases were detected in the X-ray diffraction analysis of the single crystals of $MgVO_3$. On the other hand, it was difficult to obtain a pure polycrystalline phase of $MgVO_3$. X-ray powder diffraction patterns show systematically the presence of a few percent of a secondary phase with the spinel structure (a = 8.40(2) Å). Careful examination of the samples in an optical microscope revealed a brown body with numerous black dotted inclusions. These black regions may be related to the secondary phase. Little is known about this phase except that it is paramagnetic down to $\sim$ 12 K and its proportion approximately corresponds to 4−7% of the total spin concentration (see below).

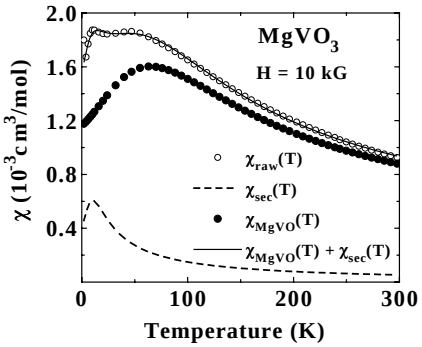

Fig. 2. The temperature dependence of the magnetic susceptibility of a 137 mg $MgVO_3$ polycrystalline sample (open circles). Solid circles, dashed curve and solid curve represent the $MgVO_3$ calculated susceptibility $\chi_{\rm MgVO}(T)$, – the secondary phase calculated susceptibility $\chi_{\rm sec}(T)$ and the sum of $\chi_{\rm MgVO}(T)$ and $\chi_{\rm sec}(T)$, respectively (see text).

Magnetic measurements and electron spin resonance experiments were carried out both on polycrystalline samples and on single crystals. X-band spectra were obtained using a Bruker ESP300 spectrometer equipped with a continuous He flow cryostat that allows temperature scans between 4 and 300 K. The temperature variation of the magnetization was measured between 2 and 300 K with a quantum design SQUID magnetometer.

4 Results

4.1 Magnetic properties

Figure 2 shows the temperature variation of the magnetic susceptibility of a 137 mg polycrystalline sample of $MgVO_3$ measured under an applied field of 10 kG. Two maxima can be seen in the measured $\chi(T)$ curve: a narrow one at approximately 12 K and a much broader one around 65 K. Note that the relative heights of these maxima depends on the sample fabrication conditions. It seems that the measured $\chi(T)$ is the susceptibility of a mixture of two distinct magnetic phases. Therefore, it is rather tempting to ascribe the 12 K maximum to the magnetic contribution of the secondary phase, as discussed in the previous section. Hereafter we develop the arguments in favor of this interpretation.

Now we consider a few simple models for $\chi(T)$ allowing a quantitative analysis of the susceptibility. The simplest one is the Curie-Weiss model. In attempting to describe the $\chi_{\rm raw}(T)$ between 130 K and 300 K by the equation $\chi_{\rm raw}(T) = \chi_{\rm V-V} + C/(T+\theta)$ the best fit is obtained with $\chi_{\rm V-V} = (6 \pm 0.03) \times 10^{-5}$ cm^3/mol,

$C = 0.36 \pm 0.02$ K cm^3/mol and $\theta = 118 \pm 1$ K indicating an antiferromagnetic behavior of a spin $S = 1/2$ system having an average g-factor $g = 1.96$. Surprisingly, this last value is in excellent agreement with the g-factor measured in ESR experiments (see next section). It is also interesting to note that the θ value is close to the value of 100 K recently reported by Chaplygin *et al.* [13].

In order to extract the contribution of $MgVO_3$ to the susceptibility, the next step is to use a model for $\chi(T)$ which has two components: one for the $MgVO_3$ phase and the other for the secondary phase. According to the crystal structure analysis, $MgVO_3$ is expected to be a quasi-one-dimensional $S = 1/2$ system. Therefore we try to fit $\chi_{\rm raw}(T)$ by the following formula representing an $S = 1/2$ infinite Heisenberg chain and a secondary phase:

$$\begin{aligned}\chi_{\rm raw}(T) &= \chi_{\rm MgVO}(T) + \chi_{\rm sec}(T) \\ &= p\frac{Ng^2\mu_{\rm B}^2}{kT}\left[\frac{A_0 + A_1X^{-1} + A_2X^{-2}}{1 + B_1X^{-1} + B_2X^{-2} + B_3X^{-3}}\right] \\ &\quad + \chi_{\rm V-V} + \chi_{\rm sec}(T) \qquad (1)\end{aligned}$$

where $g = 1.96$, $X = 2kT/J$, J being the antiferromagnetic coupling constant between the nearest neighbors defined by $H_{\rm ex} = J\sum_i \mathbf{S}_i\mathbf{S}_{i+1}$, p is a scaling constant, $\chi_{\rm sec}$ represents the secondary phase contribution, and $\chi_{\rm V-V}$ is the temperature independent susceptibility. The numerical coefficients $A_0..A_2$, $B_1..B_3$ [14] have been widely used [15,16] to reproduce the tabulated values of Bonner and Fisher calculations for the infinite $S = 1/2$ chain [17]. Note that the use of the low-temperature more precise form given by Eggert *et al.* [18] would not change the conclusions since the low-temperature part is masked by the secondary phase. For $\chi_{\rm sec}(T)$ different formulae were checked, from a simple one $\chi_{\rm sec} = C_{\rm sec}/(T + \theta_{\rm sec})$ to more sophisticated constructions allowing to simulate the 12 K maximum. Figure 2 illustrates, with one among numerous fits performed, the results we have obtained using for $\chi_{\rm sec}(T)$ the same form as for $\chi_{\rm MgVO}(T)$. Open circles, solid circles, dashed curve and solid curve represent the measured susceptibility $\chi_{\rm raw}(T)$, the susceptibility of the $MgVO_3$ phase $\chi_{\rm MgVO}(T)$, the susceptibility of the secondary phase $\chi_{\rm sec}(T)$ and the sum of $\chi_{\rm MgVO}(T)$ and $\chi_{\rm sec}(T)$, respectively. We parameterized $\chi_{\rm sec}(T)$ by $J_{\rm sec}$ and $p_{\rm sec}$ instead of J and p as in the case of the $MgVO_3$ phase. The fitting parameters are the following: $J/k = 101 \pm 0.8$ K, $p = 0.640 \pm (0.003)$, $\chi_{\rm V-V} = (2.50 \pm 0.07) \times 10^{-4}$ cm^3/mol, $J_{\rm sec}/k = 15.2 \pm 0.5$ K, $p_{\rm sec} = 0.0430 \pm (0.0001)$. One can note that the model proposed fits well the measured curve. The most important conclusions which emerge from this analysis are the following:

i) the $MgVO_3$ phase exhibits a rather pronounced $S = 1/2$ quasi-1D antiferromagnetic behavior;
ii) the value of the antiferromagnetic in-chain exchange integral can be evaluated as $J/k = 100 \pm 5$ K, quite independently of the choice of $\chi_{\rm sec}(T)$;
iii) in full agreement with the crystallographic data the magnetic proportion of the secondary phase is of the order of a few percent (typically $p_{\rm sec} = 0.03 \div 0.07$).

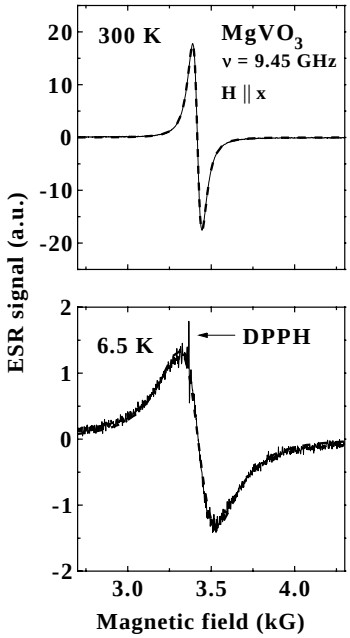

Fig. 3. Plot of two ESR spectra ($\nu = 9.45$ GHz) recorded at 300 K and 6.5 K. Continuous lines: data; dashed line: best fit to a Lorentzian profile.

We show in the next section that the contribution $\chi_{\rm MgVO}(T)$ can be easily measured in the X-band ESR experiment.

4.2 ESR study

The aim of these experiments was to obtain convincing evidence that the magnetic properties of the $MgVO_3$ crystalline phase correspond indeed to those deduced from susceptibility measurements. ESR is much more sensitive than magnetic measurements and this is why we were able to perform all standard resonance measurements in the whole temperature range 4−300 K on a small crystal of $MgVO_3$.

Two spectra recorded at 6.5 K and 300 K for $\mathbf{H}\|\mathbf{x}$ are presented in Figure 3. The best fit to a Lorentzian line shape is also shown in this figure. At 300 K (respectively 6.5 K), the agreement with this fit is good within a few percent over a magnetic field region covering $2\Delta H_{\rm p-p}$ ($\Delta H_{\rm p-p}$) on either side of the resonance field $H_{\rm r}$. $\Delta H_{\rm p-p}$ designates the peak to peak linewidth.

The spin susceptibility deduced by double integration of the ESR spectra is presented in Figure 4. While cooling the sample from 300 K, the ESR absorption first increases, passes through a maximum near $T = 60$ K and then decreases very rapidly. Fortunately, ESR does not seem to be sensitive to the presence of the secondary phase revealed by static measurements and we are therefore confident that the behavior observed in Figure 4 corresponds to that of the pure $MgVO_3$ phase. The reason for the absence of an ESR signal from the secondary phase probably resides in the fact that the corresponding vanadium ions are in a 3+ oxidation state (*i.e.* they possess a spin $S = 1$). If, however, the V ions are in a 4+ state in this phase, an

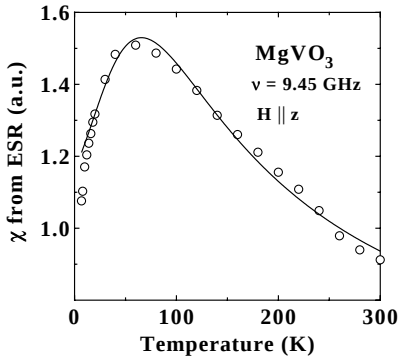

Fig. 4. Temperature variation of the double integrated ESR signal at 9.45 GHz for a single crystal sample of $MgVO_3$ for $\mathbf{H} \parallel \mathbf{z}$. The continuous line is the Bonner-Fisher formula (1) with $J/k = 100$ K.

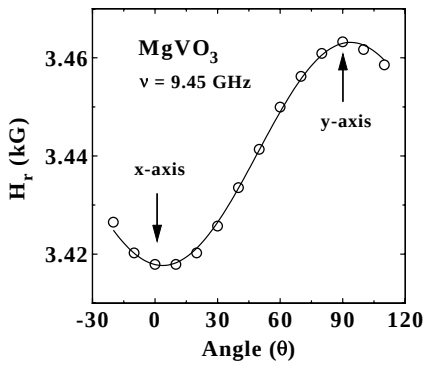

Fig. 5. Angular dependence of the ESR resonance field at $\nu = 9.45$ GHz for an $MgVO_3$ single crystal. The continuous lines correspond to a fit of the experimental data (circles) to a uniaxial anisotropy model ($g_x = g_z = 1.972(2)$, $g_y = 1.946(1)$).

excessive broadening of the signal, due to a strong spin-lattice relaxation, may also explain why this secondary phase is found ESR silent. As can be seen in Figure 4, the Bonner-Fisher susceptibility (1) for an $S = 1/2$ antiferromagnetic chain with $J/k = 100$ K fits reasonably well the experimental data.

We now detail the experimental results concerning the g-factor anisotropy. Figure 5 shows the angular dependence of the ESR resonance field ($\nu = 9.45$ GHz) at 300 K for the magnetic field rotated in the $(\mathbf{x}, \mathbf{y})$ plane. $H_{\rm r}(\theta)$ passes through two extrema near $\theta = 0°$ and $\theta = 90°$ and does not vary by more than 40 G. An axial anisotropy model was used to fit the obtained data. The angular dependence was fitted with the expression $H_{\rm r}(\theta) = g_{\rm DPPH} H_{\rm DPPH}/g(\theta)$ where

$$g^2(\theta) = g_x^2 \cos^2(\theta) + g_y^2 \sin^2(\theta) \qquad (2)$$

for $\mathbf{H}$ rotated in the $(\mathbf{x}, \mathbf{y})$ crystal plane. Good agreement is found between the data and this formula. The values of g-factors extracted from this fit are $g_x = g_z = 1.972(2)$ and $g_y = 1.946(1)$. The uniaxial anisotropy revealed by these experiments is consistent with the X-ray data.

The temperature variation of the resonance linewidth in the paramagnetic phase of $MgVO_3$ is reported in Figure 6. The different curves correspond to the magnetic

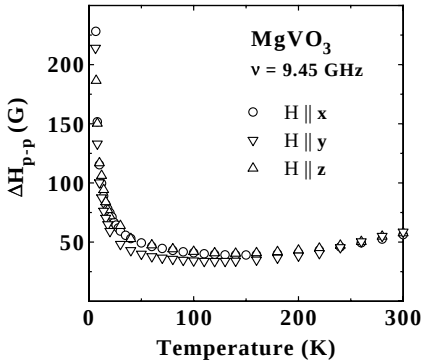

Fig. 6. Temperature dependence of the ESR linewidth $\Delta H_{\rm p-p}$ at 9.45 GHz determined for the three crystallographic directions.

field applied along the three crystallographic directions. At room temperature, the linewidth is almost isotropic ($\Delta H^{\perp}_{\rm p-p} \simeq 56.3(3)$ G, $\Delta H^{\parallel}_{\rm p-p} \simeq 58.6(3)$ G). When the temperature decreases from 300 K, the linewidth first slightly decreases and then broadens as the 3D antiferromagnetic phase transition is approached at $T_{\rm N}$. Below $T \simeq 200$ K $\Delta H_{\rm p-p}$ becomes anisotropic. The fact that the ESR linewidth shows a minimum at $T \simeq 100$ K may indicate that two different mechanisms of line broadening are operative in this temperature region. The first one is dominant at $T \ll J/k$ and is responsible for the broadening caused by 1D antiferromagnetic fluctuations in the chains. The second one affects the linewidth at $T \gg J/k$. The following empirical expression was used in order to fit $\Delta H_{\rm p-p}(T)$ over the whole temperature range studied experimentally:

$$\Delta H_{\rm p-p}(T) = C_1 + C_2\ T + C_3\ T^2 + C_4 \left[\frac{T - T_{\rm N}}{T_{\rm N}}\right]^{-C_5} \qquad (3)$$

where C_1, C_2, C_3, C_4, C_5 and $T_{\rm N}$ are parameters, C_5 being an exponent characterizing the low temperature broadening. Several models were checked:

i) zero value imposed for both linear and quadratic terms but $C_1 \neq 0$,
ii) $C_1 \neq 0$, $C_2 \neq 0$, $C_3 = 0$,
iii) $C_1 \neq 0$, $C_2 = 0$, $C_3 \neq 0$.

Among the three models, the first one is the worse since it does not predict a minimum of the linewidth at any temperature. The second one is slightly better but the agreement with experimental data is poor especially above $T = 200$ K. Finally the best fit was obtained with the third model. The parameter values extracted from such a fit are gathered in Table 1. The most important conclusion is that $MgVO_3$ orders antiferromagnetically at $T_{\rm N} = 5.2 \pm 0.5$ K. The obtained value for the exponent C_5 is not discussed here because the range over which the linewidth broadens (typically 50–250 G) is not sufficiently large: a very accurate determination of the C_5 value necessitates a linewidth increase of at least one order of magnitude. Temperature stabilization to within 0.1 K or better is also required just above $T_{\rm N}$. These points cannot be realized with the small crystals and the flow cryostat used

Table 1. Fit parameters obtained, assuming $C_2 = 0$, for the linewidth temperature variation of $MgVO_3$ sample as a function of the magnetic field direction.

Parameter	$\mathbf{H} \parallel \mathbf{x}$	$\mathbf{H} \parallel \mathbf{y}$	$\mathbf{H} \parallel \mathbf{z}$
T_N (K)	5.6(1)	5.0(1)	4.8(3)
C_1 (G)	8(2)	13(2)	16(5)
C_3 (G/K^2)	0.00033(1)	0.00040(2)	0.00032(3)
C_4 (G)	97(2)	89(2)	108(5)
C_5	0.43(2)	0.56(3)	0.53(6)

in this study. Additional work is also necessary in order to clarify the underlying mechanism of linewidth broadening in $MgVO_3$ at high temperature.

5 Discussion

Our ESR and susceptibility results show that the transition metal oxide $MgVO_3$ is a quasi-1D antiferromagnet characterized by long range order below $T_N = 5.2 \pm 0.5$ K. The existence of a magnetic transition at this temperature can be inferred from the observation of the linewidth divergence, accompanied by a vanishing of the ESR intensity at T_N. The relatively large ratio J/kT_N suggests a strong space anisotropy of the exchange interactions in $MgVO_3$. This compound is interesting from several points of view. First, the coupling constant $J/k \simeq 100$ K is easily accessible by ordinary cryogenic systems and therefore, both regimes $J \gg kT$ and $J \ll kT$ can be easily explored experimentally. This is not the case of copper oxide systems. For example, the 1D Sr_2CuO_3 [19,20] compound has a coupling constant $J/k \approx 1700$ K. Another important point is related to the g-factor anisotropy which reflects the degree of departure from an ideal Heisenberg coupling. The deduced exchange anisotropy $(\Delta g/g)^2 J \simeq 0.01$ K of V^{4+} spin in $MgVO_3$ is sensibly smaller than the value typically obtained with Cu^{2+} low dimensional compounds.

Concerning the value of the exchange integrals, the following remarks can be made. First of all, a Néel temperature of 5.2 K implies that the coupling perpendicular to the chains is not negligible. It was argued in the context of Sr_2CuO_3 and Ca_2CuO_3 that if the couplings have very different values in the three directions, the Néel temperature should be of the order of magnitude of the intermediate coupling [21]. Now elementary quantum chemistry considerations suggest that the coupling within the planes should be much larger than perpendicular to the planes, so that this latter coupling should be of the order of a few degrees K. The other source of information is the Curie-Weiss temperature $\theta \simeq 118$ K which is linked to the exchange integrals by the following expression:

$$k\theta = \frac{2}{3} S(S+1) \sum \left(\frac{J}{2} \right). \qquad (4)$$

This formula implies for $S = 1/2$ that the sum of the exchange integrals starting from one site is $\sum (J/k) = 4\theta = 472$ K. Since each spin has two neighbors along the chain, a value $J/k = 100$ K implies quite large values of the coupling constants perpendicular to the chain. This seems to be inconsistent with the above estimate of the coupling perpendicular to the chains. There are two possibilities to explain this disagreement. The first possibility is that each spin is coupled to three spins in each of the neighboring chains. This is quite reasonable from a quantum chemistry point of view. As a result, the coupling between the chains is frustrated, and a Néel temperature of 5.2 K requires somewhat larger values of the exchange integrals perpendicular to the chains. The other possibility is that the coupling along the chains is indeed larger than deduced from the fit of the obtained data. It will be difficult to decide between these possibilities until larger single crystals are available.

We acknowledge useful discussions with D. Khomskii and A.B. van Oosten.

References

1. L.J. de Jongh, A.R. Miedema, Adv. Phys. **23**, 1 (1974).
2. M. Steiner, J. Villain, C.G. Windsor, Adv. Phys. **25**, 87 (1976).
3. F.D.M. Haldane, Phys. Lett. A **93**, 464 (1983); F.D.M. Haldane, Phys. Rev. Lett. **50**, 1153 (1983).
4. For a review oriented toward ladder systems see E. Dagotto, T.M. Rice, Science **271**, 618 (1996).
5. A.N. Vasil'ev, A.I. Smirnov, M. Isobe, Y. Ueda, Phys. Rev. B **56**, 5065 (1997).
6. M. Lohmann, A. Loidl, M. Klemm, G. Obermeier, S. Horn, Solid State Commun. **104**, 649 (1997).
7. D.C. Johnston, J.W. Johnson, D.P. Goshorn, A.P. Jacobson, Phys. Rev. B **35**, 219 (1987).
8. A.W. Garrett, S.E. Nagler, D.A. Tennant, D.C. Sales, T. Barnes, Phys. Rev. Lett. **79**, 745 (1997).
9. Y. Ueda, M. Isobe, J. Magn. Magn. Mater. **177-181**, 741 (1998).
10. P. Millet, C. Satto, J. Bonvoisin, B. Normand, K. Penc, M. Albrecht, F. Mila, Phys. Rev. B **57**, 5005 (1998).
11. S. Taniguchi, T. Nishikawa, Y. Yasui, Y. Kobayashi, M. Sato, T. Nishioka, M. Kontani, K. Sano, J. Phys. Soc. Jpn **6**, 2758 (1995).
12. J.C. Bouloux, I. Milosevic, J. Galy, J. Solid State Chem. **16**, 393 (1976).
13. I. Chaplygin, R. Hayn, K. Koepernik, `cond-mat/9906385`
14. $A_0 = 0.25$, $A_1 = 0.14995$, $A_2 = 0.30094$, $B_1 = 1.98620$, $B_2 = 0.68854$, $B_3 = 6.06260$.
15. M. Isobe, Y. Ueda, J. Phys. Soc. Jpn **65**, 1178 (1996).
16. G. Liu, J. E. Greedan, J. Solid State Chem. **103**, 139 (1993).
17. J.C. Bonner, M.E. Fisher, Phys. Rev. **135**, A640 (1964).
18. S. Eggert, I. Affleck, M. Takahashi, Phys. Rev. Lett. **73**, 332 (1994).
19. T. Ami, M.K. Crawford, R.L. Harlow, Z.R. Wang, D.C. Johnston, Q. Huang, R.W. Erwin, Phys. Rev. B **51**, 5994 (1995).
20. S. Eggert, Phys. Rev. B **53**, 5116 (1996).
21. A.B. van Oosten, F. Mila, Chem. Phys. Lett. **295**, 359 (1998).